Astronomy & Astrophysics manuscript no. HSfits2023FY3
October 16, 2023

When the horseshoe fits: Characterizing 2023 FY_3 with the 10.4 m Gran Telescopio Canarias and the Two-meter Twin Telescope⋆

R. de la Fuente Marcos[1], C. de la Fuente Marcos[2], J. de León[3,4], M. R. Alarcon[3,4], J. Licandro[3,4], M. Serra-Ricart[3,4,5], D. García-Álvarez[6,3], and A. Cabrera-Lavers[6,3,4]

[1] AEGORA Research Group, Facultad de Ciencias Matemáticas, Universidad Complutense de Madrid, Ciudad Universitaria, E-28040 Madrid, Spain
[2] Universidad Complutense de Madrid, Ciudad Universitaria, E-28040 Madrid, Spain
[3] Instituto de Astrofísica de Canarias (IAC), C/ Vía Láctea s/n, E-38205 La Laguna, Tenerife, Spain
[4] Departamento de Astrofísica, Universidad de La Laguna, Avda. Astrofísico Francisco Sánchez, E-38206 La Laguna, Tenerife, Spain
[5] Light Bridges S.L., Avda. Alcalde Ramírez Bethencourt, 17, E-35004, Las Palmas de Gran Canaria, Canarias, Spain
[6] GRANTECAN, Cuesta de San José s/n, E-38712 Breña Baja, La Palma, Spain

Received 7 August 2023 / Accepted 12 October 2023

ABSTRACT

Context. The Arjuna asteroid belt is loosely defined as a diverse group of small asteroids that follow dynamically cold, Earth-like orbits. Most of them are not actively engaged in resonant, co-orbital behavior with Earth. Some of them experience temporary but recurrent horseshoe episodes. Objects in horseshoe paths tend to approach Earth at low velocity leading to captures as Earth's temporary satellites or mini-moons. Four such objects have already been identified: 1991 VG, 2006 RH_{120}, 2020 CD_3, and 2022 NX_1. Here, we focus on 2023 FY_3, a recent finding whose trajectory might have co-orbital status and perhaps lead to temporary captures.
Aims. We want to determine the physical properties of 2023 FY_3 and explore its dynamical evolution.
Methods. We carried out an observational study of 2023 FY_3 using the OSIRIS camera spectrograph at the 10.4 m Gran Telescopio Canarias, to derive its spectral class, and time-series photometry obtained with QHY411M cameras and two units of the Two-meter Twin Telescope to investigate its rotational state. *N*-body simulations were also performed to examine its possible resonant behavior.
Results. The visible reflectance spectrum of 2023 FY_3 is consistent with that of an S-type asteroid; its light curve gives a rotation period of 9.3±0.6 min with an amplitude of 0.48±0.13 mag. We confirm that 2023 FY_3 roams the edge of Earth's co-orbital space.
Conclusions. Arjuna 2023 FY_3, an S-type asteroid and fast rotator, currently exhibits horseshoe-like resonant behavior and experienced mini-moon engagements of the temporarily captured flyby type in the past that may repeat in the future. The spectral type result further confirms that mini-moons are a diverse population in terms of surface composition.

Key words. minor planets, asteroids: general – minor planets, asteroids: individual: 2023 FY_3 – techniques: spectroscopic – techniques: photometric – methods: numerical – celestial mechanics

1. Introduction

Rabinowitz et al. (1993) pointed out that the path followed by the Earth–Moon system is strewn with debris in the form of small asteroids. In fact, the heliocentric orbits of these objects outline a slender torus known as the Arjuna asteroid belt (Cowen 1993; Scotti et al. 1994). They constitute a peculiar subclass within the near-Earth asteroid (NEA) population as they follow dynamically cold, Earth-like orbits (see for example Brasser & Wiegert 2008; de la Fuente Marcos & de la Fuente Marcos 2013, 2015a). Most Arjunas do not experience resonant behavior with Earth, but the Arjuna orbital domain includes Earth's co-orbital zone that roughly spans the interval of semimajor axis, a, (0.994, 1.006) au with eccentricity, e, values less than ∼0.2 (see for example de la Fuente Marcos & de la Fuente Marcos 2018b).

Although the Arjunas are the closest asteroid population to Earth, the first members of this class were only found a few decades ago (Rabinowitz et al. 1993). Their small sizes and narrow visibility windows make them difficult to study. Therefore, our current understanding of the origin and evolution of this population is still very limited, yet members of this class share the highest economic (mining) and scientific (sample retrieval) interests (see for example Sonter 1997; García Yárnoz et al. 2013; Bazzocchi & Emami 2018). Moreover, and not less important, Arjunas may evolve dynamically into impactors (see for example Sánchez-Lozano et al. 2020). Slowly but steadily, NEA surveys are uncovering the true extent and complexity of this population.

Here, we focus on 2023 FY_3, a recent discovery whose orbit might be compatible with present-day co-orbital status, lead to temporary captures, and perhaps an impact. This paper is organized as follows. In Sect. 2, we outline the dynamical context of this research, and present the data and tools used in our orbital analyses. In Sect. 3, we explore the dynamical evolution of 2023 FY_3. Details of our observations and their results are given in Sect. 4. In Sect. 5, we discuss our physical and dynamical results. Our conclusions are summarized in Sect. 6.

Send offprint requests to: R. de la Fuente Marcos, e-mail: rauldelafuentemarcos@ucm.es

⋆ Based on observations made with the Gran Telescopio Canarias (GTC) telescope, in the Spanish Observatorio del Roque de los Muchachos of the Instituto de Astrofísica de Canarias (IAC, program ID GTC31-23A) and the Two-meter Twin Telescope (TTT), in the Spanish Observatorio del Teide of the IAC (commissioning phase).

2. Dynamical context, data, and tools

Here, we review the theory needed to understand the dynamical results presented in the sections. Relevant data and tools are also discussed in this section.

2.1. Dynamics background

Most members of the Arjuna asteroid belt are passing bodies whose mean longitude relative to Earth $\lambda_r = \lambda - \lambda_\oplus$ — where λ and $\lambda_\oplus$ are the mean longitudes of the object and Earth, respectively — circulates or oscillates freely in the interval (0, 360)°; $\lambda = M + \Omega + \omega$, where M is the mean anomaly, Ω is the longitude of the ascending node, and ω is the argument of perihelion (see for example Murray & Dermott 1999). However, some others are subjected to the 1:1 mean-motion resonance with our planet, going around the Sun in almost exactly one orbital period of Earth, and experiencing temporary and sometimes recurrent libration of λ_r as this critical angle oscillates about well-defined values (see for example Dermott & Murray 1981; Morais & Morbidelli 2002; Christou & Georgakarakos 2021; Qi & Qiao 2022; Di Ruzza et al. 2023).

Among Earth co-orbitals, the most numerous group includes those objects whose λ_r librates about 180° as they roam Earth's Lagrangian point L_3, following horseshoe paths relative to our planet (see for example Hollabaugh & Everhart 1973; Ćuk et al. 2012; Kaplan & Cengiz 2020). In the classical case, the semiamplitude of this libration is <180°, but > 90°. Although the existence of these objects was first considered by Brown (1911), it took time to find and confirm the first ones hosted by Earth, 54509 YORP (2000 PH_5) (Wiegert et al. 2002) and 2002 AA_{29} (Connors et al. 2002). Additional examples were identified soon after (Brasser et al. 2004).

Minor bodies following horseshoe paths can approach Earth from behind (evening sky) or from the front (morning sky). Sometimes the relative velocity near perigee is close to or under 1 km s^{-1} leading to temporary captures. Following Fedorets et al. (2017), if an object manages to complete at least one full revolution around Earth while bound (negative geocentric energy, Carusi & Valsecchi 1979), it becomes a temporarily captured orbiter, and if it does not, a temporarily captured flyby. A similar terminology was used by Everhart (1973) within the context of temporary satellite captures by Jupiter and Saturn.

Temporarily captured small bodies are often referred to as mini-moons. Four such objects have already been identified: 1991 VG (Tancredi 1997; de la Fuente Marcos & de la Fuente Marcos 2018a), 2006 RH_{120} (Kwiatkowski et al. 2009), 2020 CD_3 (Bolin et al. 2020; de la Fuente Marcos & de la Fuente Marcos 2020; Fedorets et al. 2020a; Naidu et al. 2021), and 2022 NX_1 (de la Fuente Marcos et al. 2023). Temporarily captured orbiters — such as 2006 RH_{120} and 2020 CD_3 — have the greatest scientific and commercial value (Jedicke et al. 2018), and they may be found on a yearly basis by upcoming surveys (Fedorets et al. 2020b). In general, Arjuna-type objects are expected to be found in significant numbers by future surveys, such as LSST (see for example Schwamb et al. 2023).

2.2. Data, data sources, and tools

Asteroid 2023 FY_3 was found on March 25, 2023, at G=18.2 mag by K. W. Wierzchos observing for the Catalina Sky Survey (CSS)[1] using 0.68-m Schmidt and a 10K CCD camera (Christensen et al. 2023).[2] Table 1 shows its latest orbit determination, which is compatible with that of a NEA of the Aten dynamical class. It was retrieved from Jet Propulsion Laboratory's (JPL) Small-Body Database (SBDB)[3] provided by the Solar System Dynamics Group (SSDG, Giorgini 2011, 2015).[4] The orbit determination is referred to standard epoch JD 2460000.5 TDB, which is also the origin of time in most calculations presented here. The Earth impact risk computed by JPL's Sentry System[5] (Chamberlin et al. 2001; Chodas 2015) for the current orbit determination is low but not zero for impacts in 2114 and 2116.[6]

Table 1. Values of the heliocentric Keplerian orbital elements and their respective 1σ uncertainties of 2023 FY_3.

Orbital parameter		value±1σ uncertainty
Semimajor axis, a (au)	=	0.997747±0.000003
Eccentricity, e	=	0.0435119±0.0000007
Inclination, i (°)	=	0.24414±0.00002
Longitude of the ascending node, Ω (°)	=	26.393±0.003
Argument of perihelion, ω (°)	=	65.680±0.006
Mean anomaly, M (°)	=	58.718±0.003
Perihelion distance, q (au)	=	0.954333±0.000002
Aphelion distance, Q (au)	=	1.041161±0.000003
Absolute magnitude, H (mag)	=	29.0±0.4

Notes. The orbit determination of 2023 FY_3 is referred to epoch JD 2460000.5 (2023-Feb-25.0) TDB (Barycentric Dynamical Time, J2000.0 ecliptic and equinox), and it is based on 177 observations with a data-arc span of 30 d (solution date, May 6, 2023, 05:48:29 PDT). Source: JPL's SSDG SBDB.

As of July 9, 2023 and out of 178 known NEAs included in JPL's SBDB with $a \in [0.99, 1.01]$ au, 2023 FY_3 has the second lowest value of the orbital inclination, 0.°24, and the eighth lowest value of e, 0.044 (all data referred to epoch JD 2460000.5 TDB). These extreme values place 2023 FY_3 among the dynamically coldest group of known NEAs close to Earth's path. Among those, it is also the third smallest known, with H = 29 mag that for a visual albedo of 0.223 (see Sect. 4.1) corresponds to a size of about 5 m. Minor bodies with such properties are intrinsically difficult to discover. Asteroids that small could be produced through subcatastrophic impacts (see for example Durda et al. 2007), be released from a larger parent asteroid during very close encounters with planets following tidal disruption (see for example Schunová et al. 2014), or due to the action of the Yarkovsky–O'Keefe–Radzievskii–Paddack (YORP) mechanism (see for example Bottke et al. 2006). However, such properties are also compatible with those of objects with an artificial or lunar-ejecta origin.

The past and future orbital evolution of an object whose orbit determination is somewhat uncertain and that experiences close approaches to the Earth–Moon system that may lead to an impact has to be studied in statistical terms based on the analysis of results from a representative sample of N-body calculations that also take into account the uncertainties in the orbit determination (see for example de la Fuente Marcos & de la Fuente Marcos 2018a, 2020). To this end, we performed N-body simulations using a direct N-body code written by Aarseth

[1] https://www.lpl.arizona.edu/css/css_facilities.html

[2] https://www.minorplanetcenter.net/mpec/K23/K23FD8.html

[3] https://ssd.jpl.nasa.gov/tools/sbdb_lookup.html#/

[4] https://ssd.jpl.nasa.gov/

[5] https://cneos.jpl.nasa.gov/sentry/

[6] https://cneos.jpl.nasa.gov/sentry/details.html#?des=2023%20FY3

(2003) that implements the Hermite integration scheme formulated by Makino (1991). This software is publicly available from the website of the Institute of Astronomy of the University of Cambridge.[7] Technical details and relevant results from this code were discussed by de la Fuente Marcos & de la Fuente Marcos (2012). Our calculations were carried out in an ecliptic coordinate system with the X-axis pointing toward the Vernal Equinox and in the ecliptic plane, the Z-axis perpendicular to the ecliptic plane and pointing northward, and the Y-axis perpendicular to the previous two and defining a right handed set. Our physical model included the perturbations by the eight major planets, the Moon, the barycenter of the Pluto-Charon system, and the three largest asteroids, (1) Ceres, (2) Pallas and (4) Vesta. The input data required to perform the calculations described below were retrieved from JPL's SBDB and SSDG `Horizons` on-line Solar system data and ephemeris computation service,[8] using tools provided by the `Python` package `Astroquery` (Ginsburg et al. 2019) and its `HorizonsClass` class.[9] The retrieved initial positions and velocities (see for example Appendix A) are based on the DE440/441 planetary ephemeris (Park et al. 2021).

3. Dynamical results

The orbit determination of 2023 FY_3 in Table 1 places this object close to the edge of Earth's co-orbital zone and well within the Arjuna orbital realm, $a \in [0.99, 1.01]$ au (see for example Margot & Nicholson 2003; Connors & Innanen 2004). Figure 1 shows the short-term evolution of the nominal orbit determination in Table 1. The right panel confirms that 2023 FY_3 is currently subjected to the 1:1 mean-motion resonance with Earth and exhibits horseshoe-like resonant behavior as the value of λ_r librates about 180°. However, the left panel shows that the path followed by 2023 FY_3 in a heliocentric frame of reference rotating with Earth is not the classical horseshoe described by for example Hollabaugh & Everhart (1973) as the object loops around Earth before receding.

However and considering the uncertainties in Table 1, how robust is the horseshoe-like resonant behavior observed? Figure 2 shows the results of the evolution of relevant control orbits that are gradually more separated from the nominal one. All the control orbits confirm the current co-orbital status of 2023 FY_3 as well as its horseshoe-like resonant behavior. The figure also shows that the orbital evolution of 2023 FY_3 is rather chaotic as its past becomes unpredictable for times earlier than 1914 (over 109 yr ago) but also into the future, beyond 2044 (or about 21 yr from now). This asymmetry is the result of two close encounters with the Earth–Moon system; the future flyby will take place on March 28, 2044, at 0.00925 au (Earth's Hill radius is 0.0098 au) with a relative velocity of 1.29 km s^{-1}.

The uncertainties considered above were assumed to be uncorrelated. While this is a valid assumption when the orbit determination is precisely computed — in other words, when it is based on a large number of high-quality observations spanning a long time interval — it is certainly not expected to be true for the orbit in Table 1. In the case of 2023 FY_3, any two orbital elements may vary with each other and this issue can be properly accounted for by using the covariance matrix that is diagonal when the uncertainties are uncorrelated. In order to quantify the impact of this issue on our results, we carried out additional integrations backward and forward in time of control or clone orbits with initial conditions generated by the Monte Carlo using the Covariance Matrix (MCCM) methodology described in de la Fuente Marcos & de la Fuente Marcos (2015b). These synthetic orbits are based on the nominal orbit determination in Table 1 with random noise added on each orbital element by making use of the covariance matrix and they are compatible with the observed astrometry. The covariance matrix was retrieved from JPL's SSDG SBDB by using the `Python` package `Astroquery` and its `SBDBClass`[10] class and it is referred to epoch 2460038.5 (2023-Apr-04.0) TDB that is the origin of times for the new calculations. The MCCM approach was used to generate initial positions and velocities for 10^3 control orbits that were evolved dynamically using the direct N-body code.

Figure 3 shows the result of the past and future evolution of 2023 FY_3 when the covariance matrix is factored in. The average evolution is plotted in black and in red we show the range linked to the 1σ uncertainty or the 16th and 84th percentiles. The results are consistent with those obtained under the assumption of uncorrelated uncertainties. We confirm that predictions beyond 2044 (CE) are unreliable (see the bottom panel in Fig. 3) and that the orbital evolution prior to 1914 (CE) is highly uncertain.

We have already pointed out that sometimes the relative velocity of 2023 FY_3 at perigee near to or inside the Hill radius of Earth can be close to or under 1 km s^{-1} and this may result in a negative value of the geocentric energy, leading to temporary captures. Figure 4 shows that such temporary captures might indeed occur in the near future but the simulated events take place outside the time interval in which predictions based on the current orbit determination are reliable. When longer time intervals are explored, recurrent temporary captures are observed (see Fig. 5, bottom panel). During most of the simulated time, 2023 FY_3 remains inside the Arjuna orbital domain but not engaged in 1:1 resonant behavior with Earth (see Fig. 5, top panel). Although most temporary capture events were of the temporarily captured flyby type like the one shown in Fig. 6, temporarily captured orbiter episodes were also observed.

4. Observations

This section describes the different aspects of the observational techniques and data reduction procedures used in our spectroscopic and photometric study as well as their results.

4.1. Spectroscopy

We obtained the visible spectrum of asteroid 2023 FY_3 on March 28, 2023 using the Optical System for Imaging and Low Resolution Integrated Spectroscopy (OSIRIS) camera-spectrograph (Cepa et al. 2000; Cepa 2010) at the 10.4 m Gran Telescopio Canarias (GTC), under program GTC31-23A (PI, J. de León). The telescope is located at the El Roque de Los Muchachos Observatory, in the island of La Palma (Spain) and it is managed by the Instituto de Astrofísica de Canarias. The OSIRIS[11] instrument was upgraded in January 2023, and it is now equipped with a new blue-sensitive monolithic 4k×4k pixel detector that provides a total field of view of 7.8×7.8 $arcmin^2$. We used the 1.2" slit and the R300R grism that gives a resolution of about 350 for a 0.6" slit and a dispersion of 7.74 Å $pixel^{-1}$, covering the wavelength range from 0.48 to 0.92 μm. The slit was oriented along the parallactic angle and three spectra, with a exposure time of 600 s each, were obtained with an offset of 10" in the slit

[7] http://www.ast.cam.ac.uk/~sverre/web/pages/nbody.htm
[8] https://ssd.jpl.nasa.gov/horizons/
[9] https://astroquery.readthedocs.io/en/latest/jplhorizons/jplhorizons.html
[10] https://astroquery.readthedocs.io/en/latest/jplsbdb/jplsbdb.html
[11] http://www.gtc.iac.es/instruments/osiris+/osiris+.php

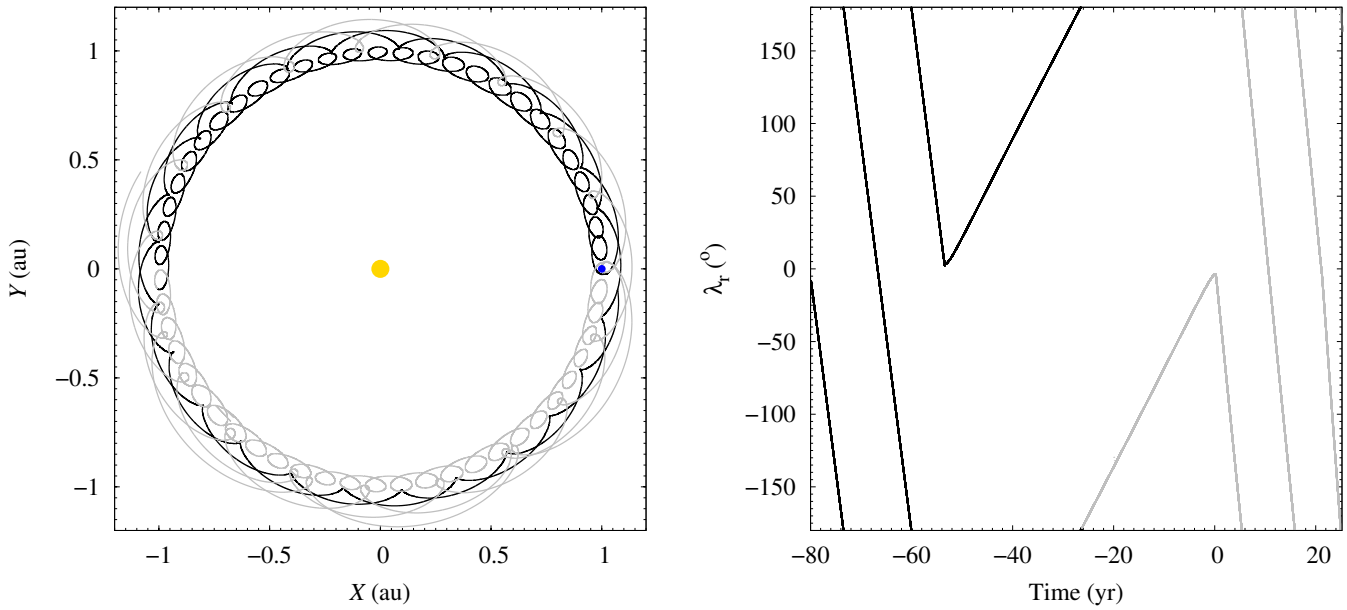

Fig. 1. Representative short-term orbital evolution of 2023 FY_3. *Left panel:* Trajectory in a heliocentric frame of reference rotating with Earth. *Right panel:* Evolution of the relative mean longitude with respect to Earth, λ_r. The figure corresponds to the evolution of the orbit determination in Table 1 in the time interval (−80, 25) yr with an output cadence of 4.383 h. The curves in black and grey correspond to the same time intervals in both panels.

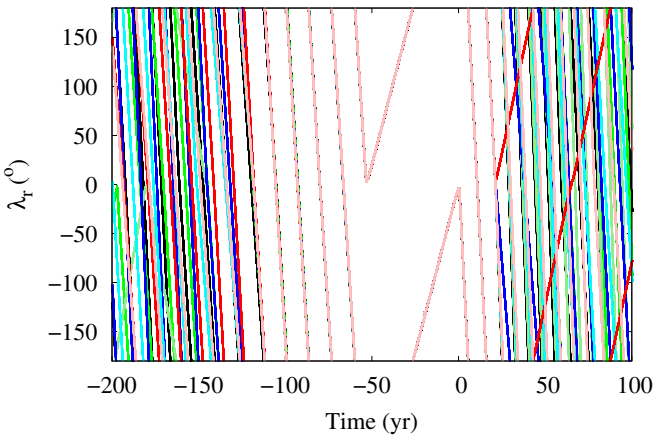

Fig. 2. Evolution of the relative mean longitude with respect to Earth, λ_r, of 2023 FY_3. The figure shows results for the nominal solution (in black) as described by the orbit determination in Table 1 and those of control orbits or clones with Cartesian state vectors (see Appendix A) separated $+3\sigma$ (in green), -3σ (in light green), $+6\sigma$ (in blue), -6σ (in cyan), $+9\sigma$ (in red), and -9σ (in pink) from the nominal values in Table A.1. The time interval (−200, 100) yr is shown. The output cadence is 4.383 h.

direction in between them. The first spectrum was acquired at 21:26 UTC, when the asteroid had an apparent visual magnitude of $m_V = 18.4$. Phase angle value and distances to the Sun and to the Earth of the target at the time of the observations were 15.5°, 1.003 au, and 0.0050 au, respectively. We also observed two solar analogue stars from the Landolt catalogue (Landolt 1992), namely SA98-978 and SA102-1081, at a similar airmass as that of the asteroid, in order to obtain its reflectance spectrum.

Data reduction was done using standard procedures. The images were bias and flat-field corrected, and sky background was subtracted. A one-dimensional spectrum was extracted from the 2D images using an aperture corresponding to the pixel where the intensity decayed to 10% of the peak value. Wavelength calibration was applied using Xe+Ne+HgAr lamps. The same reduction and extraction procedure was applied to the spectra of the asteroid and the stars. We then divided the asteroid's individual spectra by the spectra of the solar analogues, and the resulting ratios were averaged to obtain the final reflectance spectrum of 2023 FY_3 shown in Fig. 7. The error bars are associated with the standard deviation of the average.

We used the M4AST[12] online tool (Popescu et al. 2012) to taxonomically classify asteroid 2023 FY_3. This tool fits a curve to the spectrum and compares it to the taxons defined by DeMeo et al. (2009) using a χ^2 procedure. As it is shown with a grey hatch in Fig. 7, the best three matches in order of increasing χ^2 value correspond to Sq, Sr, and S-type. We also show the V-type taxon (in green), which is typical of basaltic-like composition and corresponds to the type of material that is most abundant in the surface of the Moon. Therefore, we can confidently say that asteroid 2023 FY_3 is an S-type object, which implies that it has a median albedo of $p_V = 0.223 \pm 0.073$, according to Mainzer et al. (2011). This albedo value, together with the object's absolute magnitude, provides a diameter of $D \sim 5$ m.

4.2. Time-series photometry

Photometric data were obtained on March 28, 2023 with two units of the Two-meter Twin Telescope (TTT), the TTT1 and TTT2 telescopes, located at the Teide Observatory, in the island of Tenerife (Canary Islands, Spain). These are two 0.80 m AltAz telescopes with f/4.4 and f/6.8, respectively, which were under commissioning at the time. The observations were made using the QHY411M cameras (Alarcon et al. 2023) installed in one of the Nasmyth ports of both telescopes. They are equipped with 151 Mpixel 3.76 μm sCMOS sensors, resulting in an effective FoV of 51.4×38.3 arcmin^2 and a pixel scale of 0.22" pixel^{-1}

[12] https://spectre.imcce.fr/m4ast/index.php/index/home

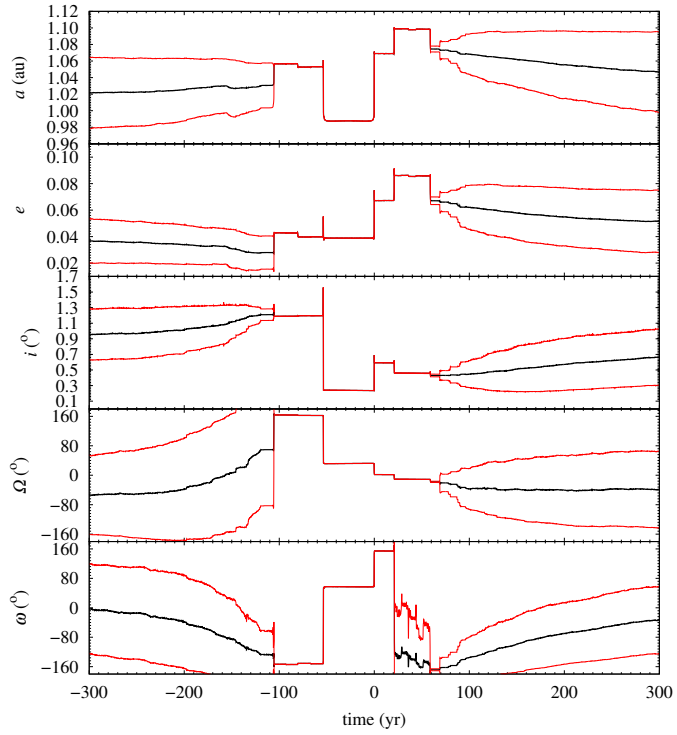

Fig. 3. Time evolution of the values of the semimajor axis (a, top panel), eccentricity (e, second to top panel), inclination (i, third to bottom panel), ascending node (Ω, second to bottom panel), and argument of perihelion (ω, bottom panel) of 2023 FY_3 according to the Monte Carlo using the Covariance Matrix (MCCM) approach as discussed by de la Fuente Marcos & de la Fuente Marcos (2015b). The panels display results of the integrations of 10^3 control orbits with initial positions and velocities generated using the MCCM method. In black, we display the average evolution of the value of the orbital element and in red we show their respective ranges described by the 1σ uncertainty or the 16th and 84th percentiles. The output cadence is 0.1 yr. The source of the input data is JPL's SBDB and Horizons system, and they are referred to epoch 2460038.5 (4-Apr-2023) TDB, which is the origin of time in this figure.

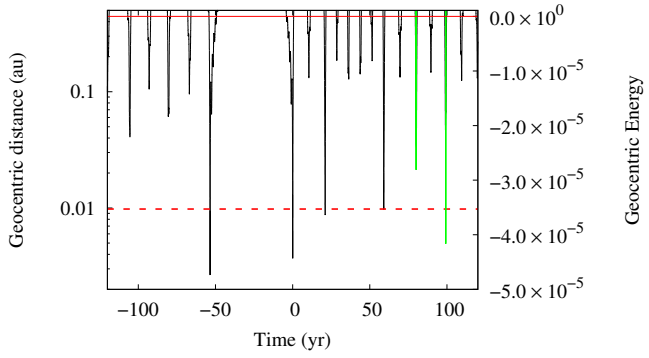

Fig. 4. Short-term time evolution of the values of the geocentric distance and energy for the nominal orbit of 2023 FY_3. The evolution of the geocentric distance is displayed in black (left side scale), the value of the Hill radius of Earth, 0.0098 au, is plotted as a red dashed line. The evolution of the geocentric energy is displayed in green (right side scale), the zero level is shown as a red continuous line. Captures take place when the value of the geocentric energy becomes negative. The unit of energy is such that the unit of mass is 1 $M_\odot$, the unit of distance is 1 au, and the unit of time is one sidereal year divided by 2π. The output cadence is 4.383 h.

in TTT1 and 33.1×24.7 arcmin^2, 0.14" pixel^{-1} in TTT2. An UV/IR-Cut CMOS-optimized filter, nearly equivalent to SDSS g′+r′, was used.

The target had an apparent visual magnitude of $m_V = 18.4$ and was moving at a rate of 14" min^{-1} at the time of observation. The observing run was divided into five 10 min observing blocks with 6.5 s continuous exposures. The median seeing during the observation period was 1.0", so the object appears slightly elongated in the images. Only two of the observing blocks had sufficient SNR to observe statistically significant variability. Hence, for the time-series photometry, two datasets observed simultaneously with both telescopes between 21:49–21:59 and 22:08–21:18 UT were included.

Data reduction was done using standard procedures. The images were bias and sky flat-field corrected. Then, the TTT2 images were binned 2×2. Aperture photometry was performed using the `Tycho Tracker`[13] software (Parrott 2020). The images were aligned with bicubic interpolation and downsampled by a factor 2 for astrometric calibration, performed using the algorithms of `Astrometry.net` (Lang et al. 2010). A fixed circular aperture of 2×FWHM in the first image was used. An outer ring located at 4×FWHM was used to estimate the sky background signal. The same apertures were used for the comparison stars, selected constraining $0.60 < (B-V) < 0.70$. The initial and final positions of the track were marked manually to prevent uncertainties in the object position coming from the ephemerides.

Photometric measurements were extracted and corrected for distance and light-time. The three-term Lomb-Scargle periodogram was obtained, with a wide peak in the power spectrum centered at a period of $P_{\rm rot} = 9.3 \pm 0.6$ min. Aliased peaks at 0.5 and 1.5 times this period are also noticeable. As uncertainty, 1σ of the Gaussian curve fitted to the exponentiated power peak was taken (VanderPlas 2018). The phased light curve is shown in Fig. 8. The amplitude of the curve computed, considering photometric errors, is 0.48±0.12 mag. Fast rotation implies intrinsic strength to resist centrifugal disruption (Pravec & Harris 2000). Therefore, 2023 FY_3 could be a coherent or monolithic body (see for example Monteiro et al. 2020). As this asteroid has a non-zero probability of colliding with Earth (see Sect. 2.2), we have to realize that small, denser objects are more likely to survive relatively unaltered the passage through the atmosphere and smash into the ground, producing local destruction. Having knowledge of this information about the bulk strength of an asteroid prior to its impact can help in optimizing mitigation strategies to face eventual damage (see for example Popescu et al. 2023). However, Sánchez & Scheeres (2014) suggested that the population of fast-rotating asteroids could include both rubble piles and monolithic boulders, because piles of rubble and dust can be held together by van der Waals forces. Considering this result, 2023 FY_3 might be made of relatively small grains and dust particles clinging on due to cohesive forces arising from weak electrostatic interparticle attractions that grow in strength for smaller particles as the forces are proportional to the contact surface area.

5. Discussion

NEA 2023 FY_3 is unlikely to have artificial origin or be lunar ejecta. This conclusion is clear when considering the spectrum in fig. 7 that corresponds to 2022 NX_1 (a former mini-moon) and those in fig. B.1 of de la Fuente Marcos et al. (2023) that includes the visible spectra of different artificial objects, and

[13] https://www.tycho-tracker.com/

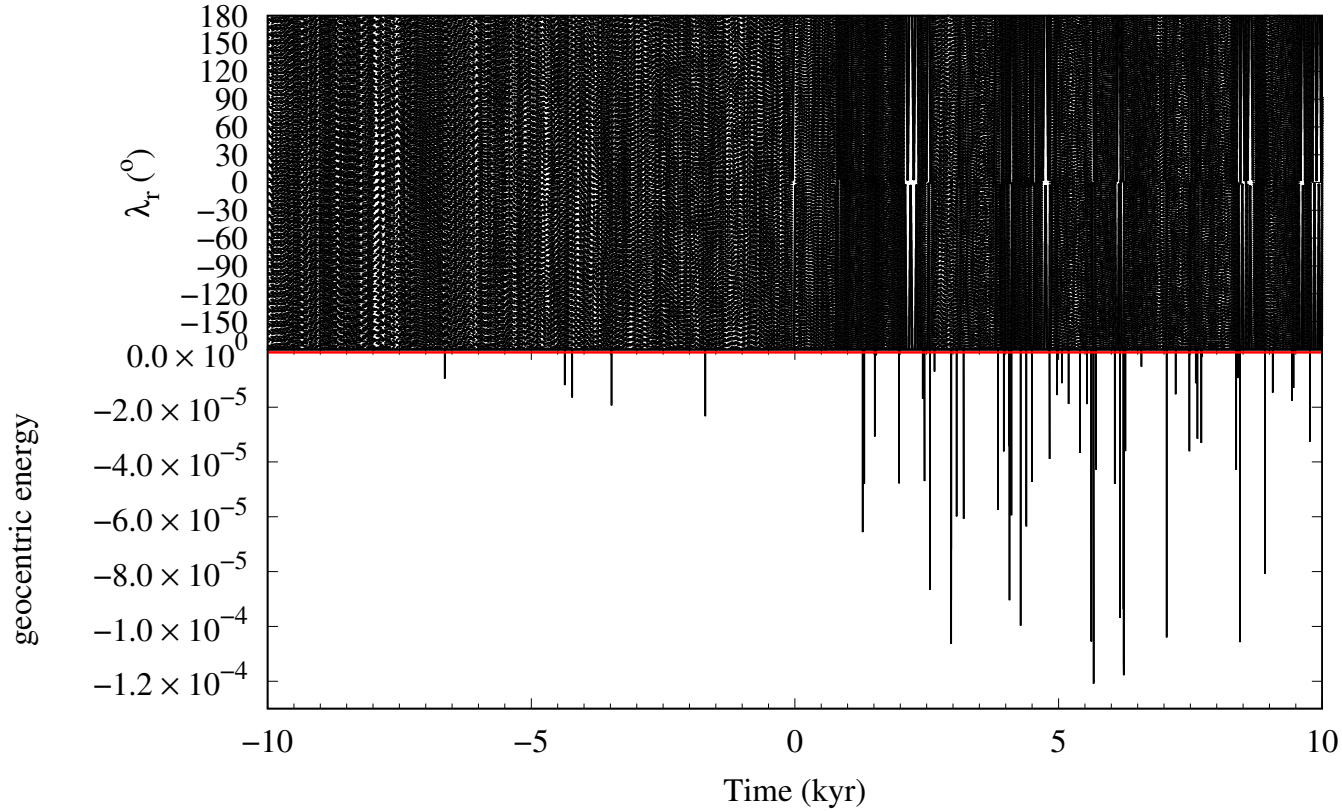

Fig. 5. Time evolution of the values of λ_r and the geocentric energy for the nominal orbit of 2023 FY_3. *Top panel:* λ_r circulates most of the time although librations are also visible. *Bottom panel:* The evolution of the geocentric energy shows that recurrent temporary captures are possible. In this figure the output cadence is 0.1 yr and only temporary captures lasting two or more months are visible. Captures take place when the value of the geocentric energy becomes negative. The unit of energy is such that the unit of mass is 1 $M_\odot$, the unit of distance is 1 au, and the unit of time is one sidereal year divided by 2π.

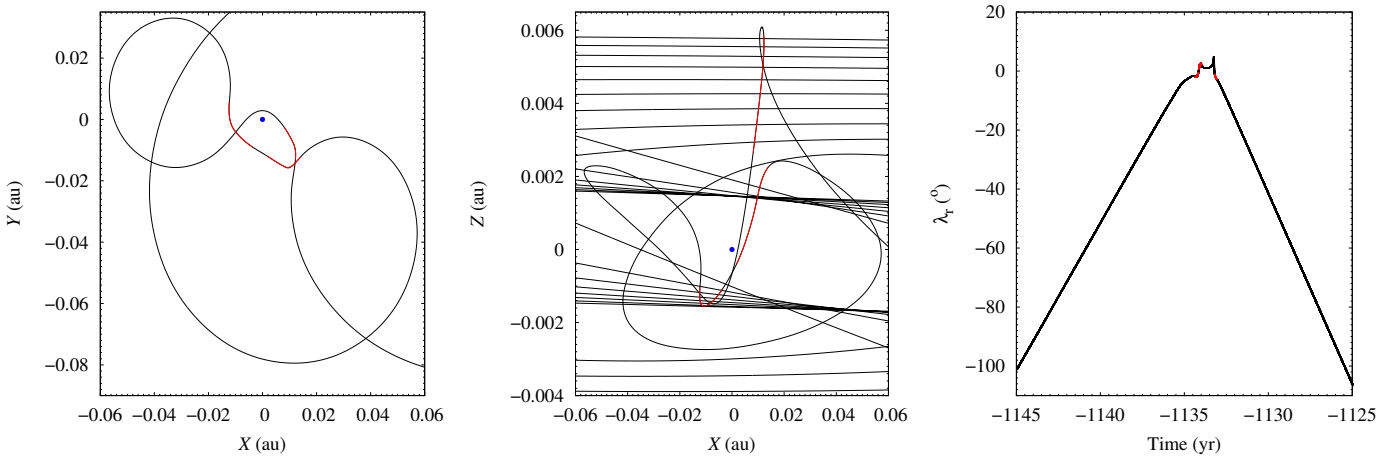

Fig. 6. Geocentric trajectory and evolution of λ_r during one double temporarily captured flyby. In this example, the curves are plotted in red when the value of the geocentric energy becomes negative. *Left panel:* The geocentric $X - Y$ evolution. *Central panel:* The geocentric $X - Z$ evolution. *Right panel:* λ_r evolution.

fig. 2 of Sharkey et al. (2021) that shows the spectrum of 469219 Kamoʻoalewa (2016 HO_3) — a co-orbital that alternates quasi-satellite and horseshoe resonant states (de la Fuente Marcos & de la Fuente Marcos 2016) — that matches those of certain Lunar materials. As pointed out above, the question of what is 2023 FY_3's origin cannot be addressed by taking into account only its present-day trajectory as described by the orbit determination in Table 1 because the reconstruction of its orbital past farther than about 100 yr ago is very uncertain. An alternative approach to answering the question is in the use of an orbital distribution model for NEAs.

The NEOMOD Simulator[14] (Nesvorný et al. 2023) was developed by numerically integrating asteroid orbits from sources in the main asteroid belt and calibrating the results on observa-

[14] https://www.boulder.swri.edu/~davidn/NEOMOD_Simulator

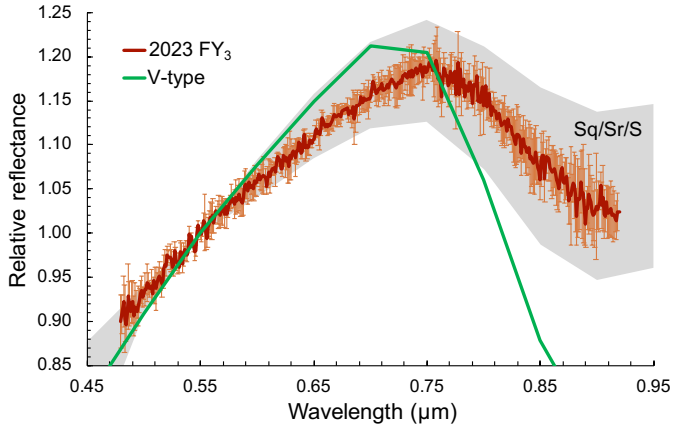

Fig. 7. Visible spectrum of asteroid 2023 FY_3 obtained with the 10.4 m Gran Telescopio Canarias (GTC) on the night of March 28, 2023. Error bars correspond to the standard deviation of the mean. The grey hatched region accounts for the three best taxonomical fits (DeMeo et al. 2009), in order of increasing χ^2: Sq, Sr, and S-type. We also show the taxon corresponding to V-types (basaltic asteroids), in green, for comparison purposes.

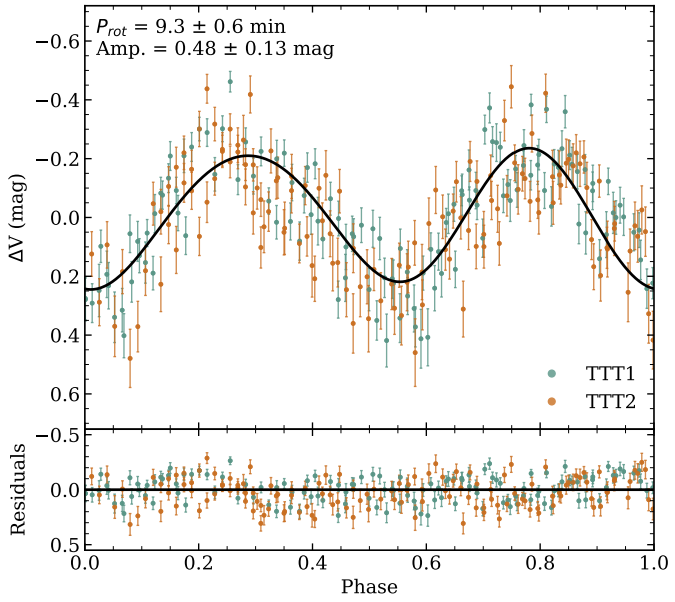

Fig. 8. Phased light curve of 2023 FY_3 derived from photometric measurements obtained by the TTT1 and TTT2 telescopes. The rotation period and amplitude of the curve are shown at the upper left.

tions of the CSS. Although the model is only strictly applicable to objects with $H \leq 28.0$ mag and 2023 FY_3 has $H = 29.0$ mag, it may provide a robust answer to the question if we assume that this object is not a fragment produced through the tidal or rotational breakup of a larger body during a close encounter with the Earth–Moon system. Considering the real number of synthetic NEAs generated by NEOMOD (input option −1) in the interval $H \in [15.0, 28.0]$ mag and the orbits most closely matching the one in Table 1, 2023 FY_3 may have an origin in the inner region of the main belt with a probability close to 70% of having been delivered through the ν_6 secular resonance and a 20% chance of coming from the 3:1 mean-motion resonance with Jupiter.

The Arjuna secondary asteroid belt is made of small bodies inserted from the main asteroid belt through resonances or produced in situ via fragmentation processes. These small asteroids follow dynamically cold, Earth-like orbits. Some of them can become co-orbitals, in particular horseshoes and quasi-satellites, but also mini-moons. The properties of this population remain poorly understood because relatively large objects are scarce and its members are seldom favorably positioned to be observed from ground-based telescopes. In addition, this region also hosts many objects that are eventually confirmed as active spacecraft or returning space debris. Spectroscopy is critical to identify false positives as pointed out by de la Fuente Marcos et al. (2023) but few Arjunas have spectral information. In addition to the few examples pointed out above, another object with available spectroscopy is the former mini-moon 2020 CD_3 that has a V-type (Bolin et al. 2020). The relatively short visibility windows of these objects make them challenging spectroscopic targets.

Thanks to the study of objects like 2023 FY_3, the historically blurred picture of the Arjuna secondary asteroid belt is now emerging somewhat clearer and a recent study concludes that Arjunas tend to have the smallest MOIDs (Minimum Orbit Intersection Distance) with Earth and the largest values of H (Deshapriya et al. 2023). In this context, 2023 FY_3 represents a rare window into the subset of the smallest NEAs, but also into the group of ephemeral Earth horseshoes. The spectral type of 2023 FY_3, when considered within the context of those of other spectroscopically characterized Arjunas (see above), its small size and rapid rotation, and its peculiar dynamics point to a fast-evolving, resonance-driven, diverse Arjuna belt whose study may provide insights into the nature of the internal structure of larger, heterogeneous asteroids (their building blocks), and the dynamical context of any planetary defense strategies, but also on the economics of in-space mineral supply procurement.

6. Summary and conclusions

In this paper, we have presented results of an observational and numerical study of the Arjuna-type asteroid 2023 FY_3 — a small Earth's co-orbital candidate — that combines several techniques. Spectroscopic observations acquired with the OSIRIS camera spectrograph at the 10.4 m GTC were used to perform a physical characterization of the object; its rotational state was investigated with time-series photometry obtained with QHY411M cameras and two units of the Two-meter Twin Telescope; and its orbital evolution was explored using N-body simulations. Our conclusions can be summarized as follows.

1. We show that 2023 FY_3 is a natural small body with a visible reflectance spectrum consistent with that of an S-type asteroid.
2. We analyzed its light curve and obtained a rotation period of 9.3±0.6 min with an amplitude of 0.48±0.13 mag, typical of small monolithic asteroids.
3. We confirm that 2023 FY_3 is currently engaged in horseshoe-like resonant behavior with Earth and experiences regular encounters with the Earth–Moon system well inside the Hill radius and at relative velocities close to 1 km s^{-1}.
4. The orbit determination of 2023 FY_3 is not robust enough to make reliable predictions of its orbital evolution beyond March 28, 2044, or reconstruct its dynamical behavior farther than about 100 yr into the past.
5. Using the NEOMOD orbital distribution model for NEAs, 2023 FY_3 may have an origin in the inner region of the main asteroid belt with a probability close to 70% of having been

delivered through the ν_6 secular resonance and a 20% chance of coming from the 3:1 mean-motion resonance with Jupiter. An origin within the Arjuna orbital realm as a result of the fragmentation in situ of a larger parent body cannot be discarded.

6. The analysis of a large sample of control orbits shows that encounters at close range and low relative velocity with the Earth–Moon system may have resulted in past temporary satellite captures that could happen again in the future. Although engagements of the temporarily captured flyby type are far more probable, temporary captured orbiter episodes are also possible.

The faint end of the small-body size function is far from being well studied (see for example Trilling et al. 2017; Heinze et al. 2021). For 15% albedo, $H = 27.6$ mag is equivalent to a size of 10 m (Heinze et al. 2021). At $H = 29.0$ mag, 2023 FY_3 is one of the smallest known asteroids with both spectroscopic characterization and rotation period determination. Its fast spinning suggests that it could be a coherent body, a single boulder or piece of rubble that came from a larger rubble-pile host, perhaps released by the YORP mechanism. Given its size and dynamical properties, the Arjuna belt may host thousands of objects like 2023 FY_3.

Acknowledgements. We thank the anonymous referee for a timely, comprehensive, and constructive report. RdlFM and CdlFM thank S. J. Aarseth for providing one of the codes used in this research and A. I. Gómez de Castro for providing access to computing facilities. JdL acknowledges support from the ACIISI, Consejería de Economía, Conocimiento y Empleo del Gobierno de Canarias and the European Regional Development Fund (ERDF) under grant with reference ProID2021010134. JdL also acknowledges financial support from the Spanish Ministry of Science and Innovation (MICINN) through the Spanish State Research Agency, under Severo Ochoa Programme 2020-2023 (CEX2019-000920-S). This work was partially supported by the Spanish 'Agencia Estatal de Investigación (Ministerio de Ciencia e Innovación)' under grant PID2020-116726RB-I00 /AEI/10.13039/501100011033. Based on observations made with the Gran Telescopio Canarias (GTC), installed at the Spanish Observatorio del Roque de los Muchachos of the Instituto de Astrofísica de Canarias, on the island of La Palma. This work is partly based on data obtained with the instrument OSIRIS, built by a Consortium led by the Instituto de Astrofísica de Canarias in collaboration with the Instituto de Astronomía of the Universidad Nacional Autónoma de Mexico. OSIRIS was funded by GRANTECAN and the National Plan of Astronomy and Astrophysics of the Spanish Government. This paper includes observations made during the commissioning of the Two-meter Twin Telescope (TTT) at the IAC's Teide Observatory that Light Bridges, SL, operates on the Island of Tenerife, Canary Islands (Spain). The Observing Time Rights (DTO) used for this research at the TTT have been provided by the Instituto de Astrofísica de Canarias. In preparation of this paper, we made use of the NASA Astrophysics Data System, the ASTRO-PH e-print server, and the MPC data server.

References

Aarseth, S. J. 2003, Gravitational N-Body Simulations (Cambridge: Cambridge University Press), 27
Alarcon, M. R., Licandro, J., Serra-Ricart, M., et al. 2023, PASP, 135, 055001
Bazzocchi, M. C. F. & Emami, M. R. 2018, Journal of Spacecraft and Rockets, 55, 37
Bolin, B. T., Fremling, C., Holt, T. R., et al. 2020, ApJ, 900, L45
Bottke, W. F., Vokrouhlický, D., Rubincam, D. P., et al. 2006, Annual Review of Earth and Planetary Sciences, 34, 157
Brasser, R., Innanen, K. A., Connors, M., et al. 2004, Icarus, 171, 102
Brasser, R. & Wiegert, P. 2008, MNRAS, 386, 2031
Brown, E. W. 1911, MNRAS, 71, 438
Carusi, A. & Valsecchi, G. B. 1979, Riunione della Societa Astronomica Italiana, 22, 181
Cepa, J., Aguiar, M., Escalera, V. G., et al. 2000, Proc. SPIE, 4008, 623
Cepa, J. 2010, Astrophysics and Space Science Proceedings, 14, 15
Chamberlin, A. B., Chesley, S. R., Chodas, P. W., et al. 2001, American Astronomical Society, DPS Meeting #33, id.41.08
Chodas, P. 2015, American Astronomical Society, DPS meeting #47, id.214.09
Christensen, E. J., Fay, D., Fazekas, J. B., et al. 2023, Minor Planet Electronic Circulars, 2023-F138
Christou, A. A. & Georgakarakos, N. 2021, MNRAS, 507, 1640
Connors, M., Chodas, P., Mikkola, S., et al. 2002, Meteoritics Planet. Sci., 37, 1435
Connors, M. & Innanen, K. 2004, AGU Spring Meeting, abstract id.P11A-04
Cowen, R. 1993, Science News, 143, 117
Ćuk, M., Hamilton, D. P., & Holman, M. J. 2012, MNRAS, 426, 3051
de la Fuente Marcos, C. & de la Fuente Marcos, R. 2012, MNRAS, 427, 728
de la Fuente Marcos, C. & de la Fuente Marcos, R. 2013, MNRAS, 434, L1
de la Fuente Marcos, C. & de la Fuente Marcos, R. 2015a, Astronomische Nachrichten, 336, 5
de la Fuente Marcos, C. & de la Fuente Marcos, R. 2015b, MNRAS, 453, 1288
de la Fuente Marcos, C. & de la Fuente Marcos, R. 2016, MNRAS, 462, 3441
de la Fuente Marcos, C. & de la Fuente Marcos, R. 2018a, MNRAS, 473, 2939
de la Fuente Marcos, C. & de la Fuente Marcos, R. 2018b, MNRAS, 473, 3434
de la Fuente Marcos, C. & de la Fuente Marcos, R. 2020, MNRAS, 494, 1089
de la Fuente Marcos, R., de León, J., de la Fuente Marcos, C., et al. 2023, A&A, 670, L10
DeMeo, F., Binzel, R. P., Slivan, S. M., et al. 2009, Icarus, 202, 160
Dermott, S. F. & Murray, C. D. 1981, Icarus, 48, 1
Deshapriya, J. D. P., Perna, D., Bott, N., et al. 2023, A&A, 674, A50
Di Ruzza, S., Pousse, A., & Alessi, E. M. 2023, Icarus, 390, 115330
Durda, D. D., Bottke, W. F., Nesvorný, D., et al. 2007, Icarus, 186, 498
Everhart, E. 1973, AJ, 78, 316
Fedorets, G., Granvik, M., & Jedicke, R. 2017, Icarus, 285, 83
Fedorets, G., Micheli, M., Jedicke, R., et al. 2020a, AJ, 160, 277
Fedorets, G., Granvik, M., Jones, R. L., et al. 2020b, Icarus, 338, 113517
García Yárnoz, D., Sanchez, J. P., & McInnes, C. R. 2013, Celestial Mechanics and Dynamical Astronomy, 116, 367
Ginsburg, A., Sipőcz, B. M., Brasseur, C. E., et al. 2019, AJ, 157, 98
Giorgini, J. 2011, in Journées Systèmes de Référence Spatio-temporels 2010, ed. N. Capitaine, 87–87
Giorgini, J. D. 2015, IAUGA, 22, 2256293
Heinze, A. N., Denneau, L., Tonry, J. L., et al. 2021, PSJ, 2, 12
Hollabaugh, M. & Everhart, E. 1973, Astrophys. Lett., 15, 1
Jedicke, R., Bolin, B. T., Bottke, W. F., et al. 2018, Frontiers in Astronomy and Space Sciences, 5, 13
Kaplan, M. & Cengiz, S. 2020, MNRAS, 496, 4420
Kwiatkowski, T., Kryszczyńska, A., Polińska, M., et al. 2009, A&A, 495, 967
Landolt, A. U. 1992, AJ, 104, 340
Lang, D., Hogg, D. W., Mierle, K., et al. 2010, AJ, 139, 1782
Mainzer, A., Grav, T., Masiero, J., et al. 2011, ApJ, 741, 90
Makino, J. 1991, ApJ, 369, 200
Margot, J. L. & Nicholson, P. D. 2003, AAS/Division of Dynamical Astronomy Meeting #34, id.06.15
Monteiro, F., Silva, J. S., Tamayo, F., et al. 2020, MNRAS, 495, 3990
Morais, M. H. M. & Morbidelli, A. 2002, Icarus, 160, 1
Murray, C. D. & Dermott, S. F. 1999, Solar system dynamics (Cambridge, UK: Cambridge University Press)
Naidu, S. P., Micheli, M., Farnocchia, D., et al. 2021, ApJ, 913, L6
Nesvorný, D., Deienno, R., Bottke, W. F., et al. 2023, AJ, 166, 55
Park, R. S., Folkner, W. M., Williams, J. G., et al. 2021, AJ, 161, 105
Parrott, D. 2020, JAAVSO, 48, 262
Popescu, M., Birlan, M., & Nedelcu, D. A. 2012, A&A, 544, A130
Popescu, M. M., Văduvescu, O., de León, J., et al. 2023, A&A, 676, A126
Pravec, P. & Harris, A. W. 2000, Icarus, 148, 12
Qi, Y. & Qiao, D. 2022, AJ, 163, 211
Rabinowitz, D. L., Gehrels, T., Scotti, J. V., et al. 1993, Nature, 363, 704
Sánchez, P. & Scheeres, D. J. 2014, Meteor. Planet. Sci., 49, 788
Sánchez-Lozano, J. M., Fernández-Martínez, M., Saucedo-Fernández, A. A., et al. 2020, Acta Astronautica, 176, 383
Schunová, E., Jedicke, R., Walsh, K. J., et al. 2014, Icarus, 238, 156
Schwamb, M. E., Jones, R. L., Yoachim, P., et al. 2023, ApJS, 266, 22
Scotti, J. V., Gehrels, T., & Rabinowitz, D. L. 1994, 160th International Astronomical Union Symposium, Asteroids, Comets, Meteors 1993, ed. A. Milani, M. Di Martino, & A. Cellino (Dordrecht, Holland: Kluwer Academic Publishers) 810, 266
Sharkey, B. N. L., Reddy, V., Malhotra, R., et al. 2021, Communications Earth and Environment, 2, 231
Sonter, M. J. 1997, Acta Astronautica, 41, 637
Tancredi, G. 1997, Celestial Mechanics and Dynamical Astronomy, 69, 119
Trilling, D. E., Valdes, F., Allen, L., et al. 2017, AJ, 154, 170
VanderPlas, J. T. 2018, ApJS, 236, 16
Wiegert, P., Connors, M., Chodas, P., et al. 2002, AGU Fall Meeting Abstracts, id.P11A-0352

Table A.1. Barycentric Cartesian state vector of 2023 FY_3: components and associated 1σ uncertainties.

Component		value$\pm 1\sigma$ uncertainty
X (au)	=	$-8.953431535257687\times10^{-1}\pm8.55816440\times10^{-8}$
Y (au)	=	$4.096847623022677\times10^{-1}\pm5.53879427\times10^{-7}$
Z (au)	=	$3.456629464841657\times10^{-3}\pm1.94403735\times10^{-7}$
V_X (au/d)	=	$-7.986119960857692\times10^{-3}\pm8.12817244\times10^{-9}$
V_Y (au/d)	=	$-1.568041957560417\times10^{-2}\pm1.81148808\times10^{-8}$
V_Z (au/d)	=	$-4.465281351986577\times10^{-5}\pm7.02163094\times10^{-9}$

Notes. Data are referred to epoch JD 2460000.5, which corresponds to 0:00 on February 25, 2023, TDB (J2000.0 ecliptic and equinox). Source: JPL's `Horizons`.

Appendix A: Input data

Here, we include the barycentric Cartesian state vector of NEA 2023 FY_3. This vector and its uncertainties were used to perform some of the calculations discussed above and to generate the figure that displays the time evolution of the critical angle, λ_r (Fig. 2). For example, a new value of the X component of the state vector is computed as $X_c = X + \sigma_X\, r$, where r is an univariate Gaussian random number, and X and σ_X are the mean value and its 1σ uncertainty in Table A.1.